11th AIAA/CEAS Aeroacoustics Conference, 23-25 May 2005, Monterey, CA, USA

An Analytic Green's Function for a Lined Circular Duct Containing Uniform Mean Flow (corr.)

Sjoerd W. Rienstra*

Eindhoven University of Technology, 5600 MB Eindhoven, The Netherlands.

Brian J. Tester†

University of Southampton, Southampton S017 1BJ, UK.

An analytic Green's function is derived for a lined circular duct, both hollow and annular, containing uniform mean flow, from first principles by Fourier transformation. The derived result takes the form of a common mode series. All modes are assumed to decay in their respective direction of propagation. A more comprehensive causality analysis suggests the possibility of upstream modes being really downstream instabilities. As their growth rates are usually exceptionally large, this possibility is not considered in the present study.

We show that the analytic Green's function for a lined hollow circular duct, containing uniform mean flow, is essentially identical to that used by Tester e.a. in the Cargill splice scattering model. The Green's function for the annular duct is new.

Comparisons between the numerically obtained modal amplitudes of Alonso e.a. and the present analytic results for a lined, hollow circular duct show good agreement without flow, irrespective of how many modes are included in the matrix inversion for the numerical mode amplitudes. With flow, the mode amplitudes do not agree but as the number of modes included in the matrix inversion is increased the numerically obtained modal amplitudes of Alonso e.a. appear to be converging to the present analytical result.

In practical applications our closed form analytic Green's function will be computationally more efficient, especially at high frequencies of practical interest to aero-engine applications, and the analytic form for the mode amplitudes could permit future modelling advances not possible from the numerical equivalent.

Nomenclature

a	=	duct diameter
$\mathcal{C}_m$, $\mathcal{D}_m$	=	linear combinations of Bessel functions J_m and Y_m
$\boldsymbol{e}_x$, $\boldsymbol{e}_r$, $\boldsymbol{e}_\theta$	=	unit vectors in x, r, θ-direction
E_m	=	auxiliary functions of κ
F_m, H_m, $\mathcal{F}_m$, $\mathcal{H}_m$	=	auxiliary functions of r and α
$G(\boldsymbol{x};\boldsymbol{x}_0)$	=	Green's function (in pressure)
$G_m(r,x)$	=	m-th circumferential Fourier component of $G(\boldsymbol{x};\boldsymbol{x}_0)$
$H(x)$	=	Heaviside step function
h	=	hub diameter
J_m, Y_m	=	Bessel functions of the first and second kinds of order m
m	=	circumferential modal order
M	=	Mach number
$\boldsymbol{n}$	=	unit outer normal vector at $r=1$
p, $\boldsymbol{v}$, ρ, c, ϕ	=	time-harmonic pressure, velocity, density, sound speed, potential perturbations
x, r, θ, t	=	axial, radial, azimuthal angle, time coordinate
Z_1, Z_h	=	impedance of outer, inner wall
α	=	radial modal wave number; (square root of minus) eigenvalue of Laplace operator

*Associate Professor, Department of Mathematics & Computer Science, Eindhoven University of Technology, P.O. Box 513, 5600 MB Eindhoven, The Netherlands. AIAA Member.

†Associate Consultant, ISVR, University of Southampton, Highfield, Southampton S017 1BJ, UK; AIAA Senior Member.

β = $(1 - M^2)^{1/2}$
μ = radial modal order
σ = reduced axial wave number
ω = Helmholtz number (dimensionless angular frequency)
ϖ = ω/β
Ω = $\omega - \kappa M$

I. Introduction

In some recent work, Tester e.a.[1] described the development and validation of an analytical model for the scattering of spinning modes by liner splices, originally derived by Cargill[2] and based on the Kirchhoff approximation. In his original formulation, Cargill used the hard-walled radial eigenfunctions in the Green's function for a circular duct containing uniform flow. In the recent work[1] an analytic, closed form Green's function was used that was deduced from that given by Tester[3] for a lined 2D duct containing uniform flow. This was assumed to be an approximation although it can be shown that it is a special case of the result derived by Swinbanks[4] for a lined 2D duct containing sheared flow.

More recently Alonso e.a.[5] have proposed an 'exact' Green's function based on the numerical inversion of a matrix, which is being evaluated in the course of the present work

In the current work we derive an analytic Green's function for a lined circular duct, both hollow and annular, containing uniform mean flow, from first principles, and show that the hollow version is essentially identical to that used in reference [1]. Comparisons are presented with the 'numerical' Green's function of Alonso e.a..[5,6]

We will assume for now that all modes are decay in their respective direction of propagation. More comprehensive causality analyses,[3,7,8] suggests the possibility that one (or two in case of an annular duct) upstream-running modes are really downstream-running instabilities. We will show that any suspected mode, if desired, may be easily included as an instability in the present format, but since their growth rates are usually exceptionally large, this possibility is not further explored in the present study.

II. The problem

Consider a cylindrical duct of radius $a > 0$ (possibly annular with inner radius ah), a mean flow of subsonic Mach number M, sound speed c_0 and density ρ_0 and harmonic pressure and velocity perturbations $\tilde{p}$ of angular frequency $\tilde{\omega}$. We make dimensionless

$$\tilde{\boldsymbol{x}} = x a, \quad \tilde{t} = t a/c_0, \quad \tilde{\omega} = \omega c_0/a, \, \tilde{p} = \rho_0 c_0^2 \,\mathrm{Re}(p\, \mathrm{e}^{\mathrm{i}\omega t}). \tag{1}$$

The Greens function $G(\boldsymbol{x}; \boldsymbol{x}_0)$ is represented by the pressure field $p(\boldsymbol{x})$ that is excited by a point source at $\boldsymbol{x}_0$, and satisfies the equation

$$\nabla^2 G - \Big(\mathrm{i}\omega + M\frac{\partial}{\partial x}\Big)^2 G = \delta(\boldsymbol{x} - \boldsymbol{x}_0). \tag{2}$$

Note that we use the

$$\mathrm{e}^{\mathrm{i}\omega t} \text{ - convention.} \tag{3}$$

The Ingard-Myers impedance boundary condition[9,10] with flow, a linear relation between pressure and velocity, becomes in terms of the pressure at $r = 1$

$$\Big(\mathrm{i}\omega + M\frac{\partial}{\partial x}\Big)^2 G + \mathrm{i}\omega Z_1 \frac{\partial G}{\partial r} = 0 \quad \text{at} \quad r = 1. \tag{4}$$

For a hollow duct finiteness of G is assumed at $r = 0$. For an annular duct we have at the inner wall $r = h$

$$\Big(\mathrm{i}\omega + M\frac{\partial}{\partial x}\Big)^2 G - \mathrm{i}\omega Z_h \frac{\partial G}{\partial r} = 0 \quad \text{at} \quad r = h. \tag{5}$$

Finally, we adopt radiation conditions that says that we only accept solutions that radiate away from the source position $\boldsymbol{x}_0$.

III. Solution

A. The hollow duct

We represent the delta-function by a generalised Fourier series in ϑ and Fourier integral in x

$$\delta(\boldsymbol{x}-\boldsymbol{x}_0)=\frac{\delta(r-r_0)}{r_0}\frac{1}{2\pi}\int_{-\infty}^{\infty}\mathrm{e}^{-\mathrm{i}\kappa(x-x_0)}\,\mathrm{d}\kappa\,\frac{1}{2\pi}\sum_{m=-\infty}^{\infty}\mathrm{e}^{-\mathrm{i}m(\vartheta-\vartheta_0)}. \tag{6}$$

where $0<r_0<1$, and write accordingly

$$G(x,r,\vartheta;x_0,r_0,\vartheta_0)=\sum_{m=-\infty}^{\infty}\mathrm{e}^{-\mathrm{i}m(\vartheta-\vartheta_0)}\,G_m(r,x)=\sum_{m=-\infty}^{\infty}\mathrm{e}^{-\mathrm{i}m(\vartheta-\vartheta_0)}\int_{-\infty}^{\infty}\hat{G}_m(r,\kappa)\,\mathrm{e}^{-\mathrm{i}\kappa(x-x_0)}\,\mathrm{d}\kappa. \tag{7}$$

Substitution of (6) and (7) in (2) yields for $\hat{G}_m$

$$\frac{\partial^2\hat{G}_m}{\partial r^2}+\frac{1}{r}\frac{\partial\hat{G}_m}{\partial r}+\Big(\alpha^2-\frac{m^2}{r^2}\Big)\hat{G}_m=\frac{\delta(r-r_0)}{4\pi^2 r_0}, \tag{8}$$

with

$$\alpha^2=\Omega^2-\kappa^2,\quad \Omega=\omega-\kappa M. \tag{9}$$

This has solution

$$\hat{G}_m(r,\kappa)=A(\kappa)\,\mathrm{J}_m(\alpha r)+\tfrac{1}{8\pi}H(r-r_0)\big(\mathrm{J}_m(\alpha r_0)\,\mathrm{Y}_m(\alpha r)-\mathrm{Y}_m(\alpha r_0)\,\mathrm{J}_m(\alpha r)\big) \tag{10}$$

where J_m and Y_m denote the m-th order ordinary Besselfunctions[11] of the first and second kind, $H(r-r_0)$ denotes the Heaviside stepfunction. Use is made of the Wronskian

$$\mathrm{J}_m(x)\,\mathrm{Y}'_m(x)-\mathrm{Y}_m(x)\,\mathrm{J}'_m(x)=\frac{2}{\pi x}. \tag{11}$$

A prime denotes a derivative to the argument, x. $A(\kappa)$ is to be determined from the boundary conditions at $r=1$, which is (assuming uniform convergence) per mode

$$\mathrm{i}\Omega^2\hat{G}_m+\omega Z_1\hat{G}'_m=0\quad\text{at}\quad r=1. \tag{12}$$

A prime denotes a derivative to r. This yields

$$A=\frac{1}{8\pi}\left[\mathrm{Y}_m(\alpha r_0)-\frac{\mathrm{i}\Omega^2\,\mathrm{Y}_m(\alpha)+\omega\alpha Z_1\,\mathrm{Y}'_m(\alpha)}{\mathrm{i}\Omega^2\,\mathrm{J}_m(\alpha)+\omega\alpha Z_1\,\mathrm{J}'_m(\alpha)}\,\mathrm{J}_m(\alpha r_0)\right], \tag{13}$$

and thus

$$\hat{G}_m(r,\kappa)=\mathrm{J}_m(\alpha r_<)\frac{\mathrm{i}\Omega^2F_m(r_>,\alpha)+\omega Z_1H_m(r_>,\alpha)}{8\pi\,E_m(\kappa)}, \tag{14}$$

where

$$E_m(\kappa)=\mathrm{i}\Omega^2\,\mathrm{J}_m(\alpha)+\omega\alpha Z_1\,\mathrm{J}'_m(\alpha) \tag{15a}$$
$$F_m(r,\alpha)=\mathrm{J}_m(\alpha)\,\mathrm{Y}_m(\alpha r)-\mathrm{Y}_m(\alpha)\,\mathrm{J}_m(\alpha r) \tag{15b}$$
$$H_m(r,\alpha)=\alpha\,\mathrm{J}'_m(\alpha)\,\mathrm{Y}_m(\alpha r)-\alpha\,\mathrm{Y}'_m(\alpha)\,\mathrm{J}_m(\alpha r) \tag{15c}$$
$$r_>=\max(r,r_0) \tag{15d}$$
$$r_<=\min(r,r_0) \tag{15e}$$

By substituting the defining series we find that F_m and H_m are analytic functions of α^2, while both E_m and $\mathrm{J}_m(\alpha r_<)$ can be written as α^m times an analytic function of α^2. As a result, $\hat{G}_m(r,\kappa)$ is a meromorphic function of κ. It has isolated poles $\kappa=\kappa^{\pm}_{m\mu}$, given by $E_m(\kappa^{\pm}_{m\mu})=0$.

The final solution is found by Fourier back-transformation: close the integration contour around the lower half plane for $x > x_0$ to enclose the right propagating modes, and the upper half plane for $x < x_0$ to enclose the left propagating modes. We find

$$\left.\frac{\mathrm{d}E_m}{\mathrm{d}\kappa}\right|_{\kappa=\kappa_{m\mu}} = \omega Z_1 \,\mathrm{J}_m(\alpha_{m\mu}) \left[(\kappa_{m\mu} + \Omega_{m\mu} M)\Big(1 - \frac{m^2}{\alpha_{m\mu}^2} - \frac{\Omega_{m\mu}^4}{(\omega\alpha_{m\mu} Z_1)^2}\Big) - \frac{2\mathrm{i} M \Omega_{m\mu}}{\omega Z_1} \right], \tag{16}$$

and introduce the quantity

$$Q_{m\mu}^{\pm} = \pm \left[(\kappa_{m\mu} + \Omega_{m\mu} M)\Big(1 - \frac{m^2}{\alpha_{m\mu}^2} - \frac{\Omega_{m\mu}^4}{(\omega\alpha_{m\mu} Z_1)^2}\Big) - \frac{2\mathrm{i} M \Omega_{m\mu}}{\omega Z_1} \right], \tag{17}$$

where the $+, -$ signs apply to right, left-running modes. The integral is evaluated as a sum over the residues in the poles at $\kappa = \kappa_{m\mu}^{+}$ for $x > x_0$ and at $\kappa_{m\mu}^{-}$ for $x < x_0$, in short-hand notation given by

$$G_m(r, x) = -\tfrac{1}{4}\mathrm{i} \sum_{\mu=1}^{\infty} \mathrm{J}_m(\alpha_{m\mu} r_<) \frac{\mathrm{i}\Omega_{m\mu}^2 F_m(r_>, \alpha_{m\mu}) + \omega Z_1 H_m(r_>, \alpha_{m\mu})}{\omega Z_1 Q_{m\mu} \,\mathrm{J}_m(\alpha_{m\mu})} \,\mathrm{e}^{-\mathrm{i}\kappa_{m\mu}(x-x_0)} \tag{18}$$

where $\alpha_{m\mu} = \alpha(\kappa_{m\mu})$. From eigenvalue equation $E_m(\kappa_{m\mu}^{\pm}) = 0$ and the Wronskian (11) we obtain

$$\begin{aligned} \mathrm{i}\Omega_{m\mu}^2 F_m(r_>, \alpha_{m\mu}) + \omega Z_1 H_m(r_>, \alpha_{m\mu}) &= -\big(\mathrm{i}\Omega_{m\mu}^2 \,\mathrm{Y}_m(\alpha_{m\mu}) + \omega\alpha_{m\mu} Z_1 \,\mathrm{Y}_m'(\alpha_{m\mu})\big) \,\mathrm{J}_m(\alpha_{m\mu} r_>) \\ &= -\frac{2\omega Z_1}{\pi \,\mathrm{J}_m(\alpha_{m\mu})} \,\mathrm{J}_m(\alpha_{m\mu} r_>). \end{aligned} \tag{19}$$

So we can skip the distinction between $r_>$ and $r_<$ to achieve the soft wall modal expansion

$$G_m(r, x) = -\frac{1}{2\pi\mathrm{i}} \sum_{\mu=1}^{\infty} \frac{\mathrm{J}_m(\alpha_{m\mu} r) \,\mathrm{J}_m(\alpha_{m\mu} r_0)}{Q_{m\mu} \,\mathrm{J}_m(\alpha_{m\mu})^2} \,\mathrm{e}^{-\mathrm{i}\kappa_{m\mu}(x-x_0)} \tag{20}$$

where for $x > x_0$ the sum pertains to the right-running waves, corresponding to the modal wave numbers $\kappa_{m\mu}^{+}$ found in the lower complex half plane, and for $x < x_0$ the left-running waves, corresponding to $\kappa_{m\mu}^{-}$ found in the upper complex half plane. Equation (20) is essentially equivalent to equation (2) of [1] [a].

Only if a mode from the upper half plane is to be interpreted as a right-running instability (see [3, 7, 12]), its contribution is to be excluded from the set of modes for $x < x_0$ and included in the modes for $x > x_0$. What we essentially do is deform the integration contour into the upper half plane, so the form of the solution remains exactly the same. It may be noted that the solution is continuous everywhere, except at the source. As may be expected from the symmetry of the configuration, the clockwise and anticlockwise rotating circumferential modes are equal, i.e. $G_m(r, x) = G_{-m}(r, x)$.

B. The annular duct

By choosing suitable variables we can make the solution for the annular duct similar to the one for the hollow duct. First we introduce two independent solutions of the scaled Bessel equation, i.e. the homogeneous version of (8), by

$$\mathcal{C}_m(r; \alpha) = a \,\mathrm{J}_m(\alpha r) + b \,\mathrm{Y}_m(\alpha r), \tag{21a}$$

$$\mathcal{D}_m(r; \alpha) = c \,\mathrm{J}_m(\alpha r) + d \,\mathrm{Y}_m(\alpha r), \tag{21b}$$

[a] Unfortunately, equation (2) of Tester et al. [1] contains some minor typographical errors. The corrected form is given by

$$G(x, r, \theta | x_0, r_0, \theta_0) = -\frac{1}{2\pi\mathrm{i}} \sum_{m,n} \frac{\mathrm{J}_m(k_{rmn}^{\pm} r) \,\mathrm{J}_m(k_{rmn}^{\pm} r_0)}{\chi_{mn}^{\pm} \Lambda_{mn}^{\pm}} \exp\big[-\mathrm{i}k_{xmn}^{\pm} |x - x_0|\big] \exp\big[-\mathrm{i}m(\theta - \theta_0)\big]$$

where $k_{xmn}^{\pm} = (\mp M_x k + \chi_{mn}^{\pm})/(1 - M_x^2)$, $\chi_{mn}^{\pm} = \big(k^2 - (1 - M_x^2) k_{rmn}^{\pm\,2}\big)^{1/2}$ with $\mathrm{Im}(\chi_{mn}) \le 0$, and

$$\Lambda_{mn}^{\pm} = J_m'(k_{rmn}^{\pm})^2 + J_m(k_{rmn}^{\pm})^2 \left[1 - \frac{m^2}{k_{rmn}^{\pm\,2}} \mp \frac{2\mathrm{i} M_x (1 \mp k_{xmn}^{\pm} M_x / k)}{Z \chi_{mn}^{\pm}} \right]$$

This is equivalent to the present form if we identify $\omega = k$, $\alpha_{m\mu} = k_{rmn}$, $\kappa_{m\mu} = \pm k_{xmn}$, $(\kappa_{m\mu} + \Omega_{m\mu} M) = \pm\chi_{mn}$ and $Q_{m\mu} \,\mathrm{J}_m(\alpha_{m\mu})^2 = \chi_{mn} \Lambda_{mn}$, with the understanding that the upper sign is taken for the $x > x_0$ (i.e. the right running modes) and the lower sign for $x < x_0$ (i.e. the left running modes). This notation has the advantage that the reciprocity rule is more obvious, that is, if we exchange the observer position for the source position, the modes are the same as those we would use by simply reversing the sign of the Mach number in the above equations.

where $a\,d \neq b\,c$ and $\mathcal{C}_m$ is supposed to satisfy the inner wall boundary condition, so a and b satisfy

$$\frac{b}{a} = -\frac{\mathrm{i}\Omega^2\,\mathrm{J}_m(\alpha h) - \alpha\omega Z_h\,\mathrm{J}'_m(\alpha h)}{\mathrm{i}\Omega^2\,\mathrm{Y}_m(\alpha h) - \alpha\omega Z_h\,\mathrm{Y}'_m(\alpha h)} \tag{22}$$

Although not necessary for the final result, we will assume for convenience that $a\,d - b\,c = 1$ and

$$a = \mathrm{i}\Omega^2\,\mathrm{Y}_m(\alpha h) - \alpha\omega Z_h\,\mathrm{Y}'_m(\alpha h), \quad b = -\big(\mathrm{i}\Omega^2\,\mathrm{J}_m(\alpha h) - \alpha\omega Z_h\,\mathrm{J}'_m(\alpha h)\big).$$

$\mathcal{C}_m$ and $\mathcal{D}_m$ have now the Wronskian

$$\mathcal{C}_m\mathcal{D}'_m - \mathcal{D}_m\mathcal{C}'_m = (a\,d - b\,c)\frac{2}{\pi r} = \frac{2}{\pi r}. \tag{23}$$

The prime denotes a derivative to r. The solution of (8) that satisfies the inner wall boundary condition is

$$\hat{G}_m(r,\kappa) = A(\kappa)\mathcal{C}_m(\alpha r) + \tfrac{1}{8\pi}H(r-r_0)\big(\mathcal{C}_m(r_0;\alpha)\mathcal{D}_m(r;\alpha) - \mathcal{D}_m(r_0;\alpha)\mathcal{C}_m(r;\alpha)\big). \tag{24}$$

The boundary condition at $r = 1$ requires that A equals

$$A = \frac{1}{8\pi}\left[\mathcal{D}_m(r_0;\alpha) - \frac{\mathrm{i}\Omega^2\mathcal{D}_m(1;\alpha) + \omega Z_1\mathcal{D}'_m(1;\alpha)}{\mathrm{i}\Omega^2\mathcal{C}_m(1;\alpha) + \omega Z_1\mathcal{C}'_m(1;\alpha)}\mathcal{C}_m(r_0;\alpha)\right], \tag{25}$$

and thus

$$\hat{G}_m(r,\kappa) = \mathcal{C}_m(r_<;\alpha)\frac{\mathrm{i}\Omega^2\mathcal{F}_m(r_>,\alpha) + \omega Z_1\mathcal{H}_m(r_>,\alpha)}{8\pi\,\mathcal{E}_m(\kappa)} \tag{26}$$

where

$$\mathcal{E}_m(\kappa) = \mathrm{i}\Omega^2\mathcal{C}_m(1;\alpha) + \omega Z_1\mathcal{C}'_m(1;\alpha) \tag{27a}$$

$$\mathcal{F}_m(r,\alpha) = \mathcal{C}_m(1;\alpha)\mathcal{D}_m(r;\alpha) - \mathcal{D}_m(1;\alpha)\mathcal{C}_m(r;\alpha) \tag{27b}$$

$$\mathcal{H}_m(r,\alpha) = \mathcal{C}'_m(1;\alpha)\mathcal{D}_m(r;\alpha) - \mathcal{D}'_m(1;\alpha)\mathcal{C}_m(r;\alpha). \tag{27c}$$

In a similar way as with the hollow duct we can show that $\hat{G}_m$ is a meromorphic function in κ. Its Fourier integral that defines G_m can be evaluated in the form of a summation over the residues in $\kappa_{m\mu}$, the zeros of $\mathcal{E}_m(\kappa)$. From the defining relation $\mathcal{E}_m(\kappa_{m\mu}) = 0$ and the Wronskian we have at $\kappa = \kappa_{m\mu}$

$$\begin{aligned}\mathrm{i}\Omega^2\mathcal{F}_m(r_>;\alpha_{m\mu}) + \omega Z_1\mathcal{H}_m(r_>,\alpha_{m\mu}) &= -\big(\mathrm{i}\Omega^2\mathcal{D}_m(1;\alpha_{m\mu}) + \omega Z_1\mathcal{D}'_m(1;\alpha_{m\mu})\big)\mathcal{C}_m(r_>;\alpha_{m\mu})\\ &= -\frac{2\omega Z_1}{\pi\,\mathcal{C}_m(1;\alpha_{m\mu})}\mathcal{C}_m(r_>;\alpha_{m\mu})\end{aligned}$$

and so we have

$$\begin{aligned}G_m(r,x) &= \int_{-\infty}^{\infty}\hat{G}_m(r,\kappa)\,\mathrm{e}^{-\mathrm{i}\kappa(x-x_0)}\,\mathrm{d}\kappa\\ &= -\frac{1}{2\pi\mathrm{i}}\,\mathrm{sign}(x-x_0)\sum_{\mu=1}^{\infty}\frac{\omega Z_1}{\mathcal{E}'(\kappa_{m\mu})}\frac{\mathcal{C}_m(r;\alpha_{m\mu})\mathcal{C}_m(r_0;\alpha_{m\mu})}{\mathcal{C}_m(1;\alpha_{m\mu})}\,\mathrm{e}^{-\mathrm{i}\kappa_{m\mu}(x-x_0)}.\end{aligned}$$

By carefully substituting definitions and Wronskians we obtain

$$\begin{aligned}\left[\frac{\mathrm{d}\mathcal{E}_m}{\mathrm{d}\kappa}\right]_{\kappa=\kappa_{m\mu}} = \omega Z_1\left[\big(\kappa_{m\mu} + \Omega_{m\mu}M\big)\Big(1 - \frac{m^2}{\alpha_{m\mu}^2} - \frac{\Omega_{m\mu}^4}{(\alpha_{m\mu}\omega Z_1)^2}\Big) - \frac{2\mathrm{i}\Omega_{m\mu}M}{\omega Z_1}\right]\mathcal{C}_m(1;\alpha_{m\mu})\\ - \frac{2\omega Z_1}{\pi\,\mathcal{C}_m(1;\alpha_{m\mu})}\left[b\frac{\mathrm{d}a}{\mathrm{d}\kappa} - a\frac{\mathrm{d}b}{\mathrm{d}\kappa}\right]_{\kappa=\kappa_{m\mu}}\end{aligned}$$

Furthermore, we have

$$\left[b\frac{\mathrm{d}a}{\mathrm{d}\kappa} - a\frac{\mathrm{d}b}{\mathrm{d}\kappa}\right]_{\kappa=\kappa_{m\mu}} = \frac{2\omega^2 Z_h^2}{\pi}\left[(\kappa_{m\mu} + \Omega_{m\mu}M)\Big(1 - \frac{m^2}{\alpha_{m\mu}^2 h^2} - \frac{\Omega_{m\mu}^4}{(\alpha_{m\mu}\omega Z_h)^2}\Big) + \frac{2\mathrm{i}\Omega_{m\mu}M}{h\omega Z_h}\right]$$

and $\mathcal{C}_m(h;\alpha) = -2\omega Z_h/\pi h$. If we introduce

$$\mathcal{Q}_{m\mu}^{(1)\pm} = \pm\left[(\kappa_{m\mu}+\Omega_{m\mu}M)\Big(1-\frac{m^2}{\alpha_{m\mu}^2}-\frac{\Omega_{m\mu}^4}{(\alpha_{m\mu}\omega Z_1)^2}\Big)-\frac{2\mathrm{i}\Omega_{m\mu}M}{\omega Z_1}\right], \tag{28a}$$

$$\mathcal{Q}_{m\mu}^{(h)\pm} = \pm\left[(\kappa_{m\mu}+\Omega_{m\mu}M)\Big(1-\frac{m^2}{\alpha_{m\mu}^2h^2}-\frac{\Omega_{m\mu}^4}{(\alpha_{m\mu}\omega Z_h)^2}\Big)+\frac{2\mathrm{i}\Omega_{m\mu}M}{h\omega Z_h}\right], \tag{28b}$$

(again, the $\pm$ signs apply to right, left-running modes) we have finally in short-hand notation

$$G_m(r,x) = -\frac{1}{2\pi\mathrm{i}}\sum_{\mu=1}^{\infty}\frac{\mathcal{C}_m(r;\alpha_{m\mu})\mathcal{C}_m(r_0;\alpha_{m\mu})}{\mathcal{Q}_{m\mu}^{(1)}\mathcal{C}_m(1;\alpha_{m\mu})^2-h^2\mathcal{Q}_{m\mu}^{(h)}\mathcal{C}_m(h;\alpha_{m\mu})^2}\,\mathrm{e}^{-\mathrm{i}\kappa_{m\mu}(x-x_0)}. \tag{29}$$

C. Lorentz-type or Prandtl-Glauert transformation

We obtain for hard walls some simplification by the following Lorentz-type or Prandtl-Glauert transformation. In this case the left and right-running values of $\alpha_{m\mu}$ are symmetric, i.e. $\alpha_{m\mu}^+ = \alpha_{m\mu}^-$, while the corresponding values of $\kappa_{m\mu}$ are point symmetric in $-\omega M/(1-M^2)$. When we transform

$$\beta=\sqrt{1-M^2},\ x=\beta X,\ \omega=\beta\varpi,\ \kappa_{m\mu}^{\pm}=\frac{\pm\sigma_{m\mu}-\varpi M}{\beta},\ \Omega_{m\mu}^{\pm}=\frac{\mp M\sigma_{m\mu}+\varpi}{\beta},\ \kappa_{m\mu}+\Omega_{m\mu}M=\pm\beta\sigma_{m\mu},$$

where we can just write $\alpha_{m\mu}$ and $\sigma_{m\mu}$ without left/right distinction, we obtain

$$Q_{m\mu} = \beta\sigma_{m\mu}\Big(1-\frac{m^2}{\alpha_{m\mu}^2}\Big).$$

So altogether we have for the hollow duct

$$G_m(r,x) = -\frac{\mathrm{e}^{\mathrm{i}M\varpi(X-X_0)}}{2\pi\mathrm{i}\beta}\sum_{\mu=1}^{\infty}\frac{\mathrm{J}_m(\alpha_{m\mu}r)\,\mathrm{J}_m(\alpha_{m\mu}r_0)}{\sigma_{m\mu}\Big(1-\frac{m^2}{\alpha_{m\mu}^2}\Big)\,\mathrm{J}_m^2(\alpha_{m\mu})}\,\mathrm{e}^{-\mathrm{i}\sigma_{m\mu}|X-X_0|}. \tag{30}$$

Similarly for the annular duct we get

$$G_m(r,x) = -\frac{\mathrm{e}^{\mathrm{i}M\varpi(X-X_0)}}{2\pi\mathrm{i}\beta}\sum_{\mu=1}^{\infty}\frac{\mathcal{C}_m(r;\alpha_{m\mu})\mathcal{C}_m(r_0;\alpha_{m\mu})\,\mathrm{e}^{-\mathrm{i}\sigma_{m\mu}|X-X_0|}}{\sigma_{m\mu}\Big[\Big(1-\frac{m^2}{\alpha_{m\mu}^2}\Big)\mathcal{C}_m^2(1;\alpha_{m\mu})-h^2\Big(1-\frac{m^2}{\alpha_{m\mu}^2h^2}\Big)\mathcal{C}_m^2(h;\alpha_{m\mu})\Big]}. \tag{31}$$

Note that apart from the term $\exp[\mathrm{i}M\varpi(X-X_0)]$, G_m only depends on M^2 and $|x-x_0|$. Therefore, $|G_m(x,r)|$ is symmetric in $x-x_0$ for any subsonic Mach number.

IV. Causality

By analogy with the Helmholtz instability along an interface between two media of different velocities, it was recognised by Ffowcs Williams and Tester[3] that one mode per circumferential order (or two in annular ducts) may have the character of an instability. This means that the mode seems to propagate in the upstream direction while it decays exponentially, but in reality its direction of propagation is downstream and it increases exponentially. Tester[3] verified this conjecture by the causality argument of Briggs and Bers[13–15] (using physically reasonable frequency dependent impedance models) and found that the suspected wave indeed may be an instability, at least according to the Briggs-Bers formalism (based on tracking the modal wave numbers for complex $\omega=\omega_r+\mathrm{i}\omega_i$, with $\omega_i\to-\infty$, to see if they cross the real κ-axis). This was confirmed analytically by Rienstra in [7] for an incompressible limit of waves along an impedance of mass-spring-damper type, but now using the related causality criterion of Crighton & Leppington[16,17] (based on tracking the modal wave number for $\omega=|\omega|\exp(\mathrm{i}\varrho)$, with ϱ varying from 0 to $-\pi/2$). Rienstra & Peake [8] have shown that, although the Briggs-Bers procedure is technically not applicable and we should use the Crighton-Leppington formalism, the result of a possible instability is confirmed.

Figure 1(a) shows the behaviour of axial wave numbers $\kappa_{m\mu}$ for complex ω, with impedance model

$$Z(\omega) = R + \mathrm{i}a\omega - \frac{\mathrm{i}b}{\omega}, \tag{32}$$

which satisfies the fundamental requirements for Z to be physical and passive (see e.g. [18]), viz. Z is analytic and non-zero in $\mathrm{Im}(\omega) < 0$, $Z(\omega) = Z^*(-\omega)$ and $\mathrm{Re}(Z) > 0$. One mode crosses the real κ-axis[b] and the integration

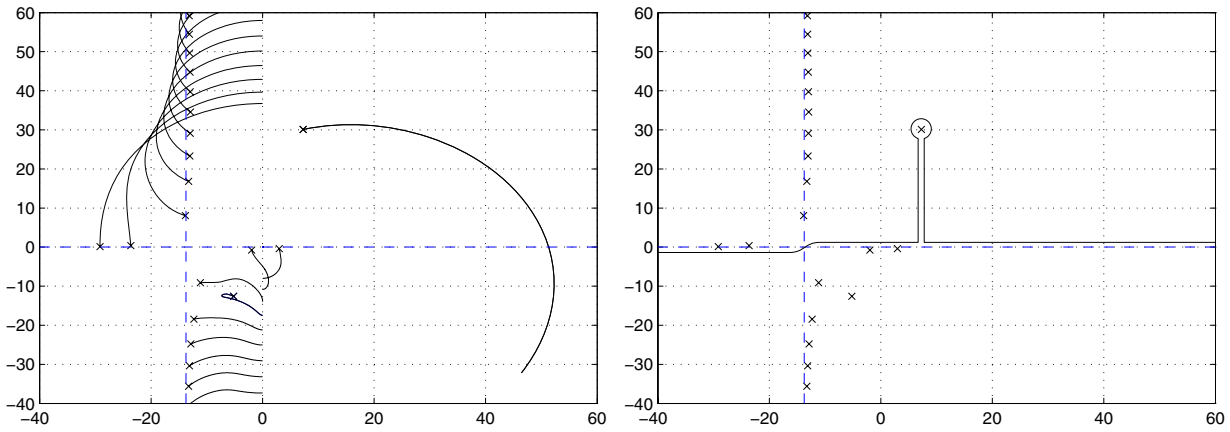

(a) Causality contours for complex ω according to the Crighton-Leppington formalism. The crosses indicate the location of the modes when $\mathrm{Im}(\omega) = 0$.

(b) The deformed intgration contour capturing the instability

Figure 1. $Z = 1 + 1.385\mathrm{i}$, $\omega = 10$, $M = 0.7$, $m = 5$, $a = 0.15$, $b = 1.15$

contour of the inverse Fourier transform should to be taken as given in figure 1(b). In other words, this mode is to be counted among the right-running modes of the lower half-plane. The results after assembling the residue contributions from below the contour for $x > x_0$ and from above the contour for $x < x_0$ are *exactly the same in form* as given by equations (20) and (29), so it is unnecessary to repeat these expressions here.

Having decided that, per m, one mode (two for annular ducts) is sometimes to be interpreted as an instability, we have cornered ourself in a difficult position. Except for impedances near the imaginary axis[7] the predicted unstable mode has invariably a large growth rate, making its presence in any physical reality at least subject to a discussion. Our linear model is based on the assumption of small perturbations. This is especially the case for the Ingard-Myers boundary condition, where the wall streamline is supposed to undergo small deflections. While it may be argued that large amplitudes of the acoustic field, away from the wall, will not immediately result into qualitatively different behaviour and are therefore acceptable to some extent, it is clear that large deflections of the wall streamline are simply unacceptable in the present model and a nonlinear model is required. Although it is possible that the instability has genuine effects acoustically in the scattering of modes at a hard-soft transition,[8] it seems futile to include the instability in a description of the field in a lined section. For this reason we have in all examples of the present paper assumed that the modes decay in their direction of propagation. In order to keep a mathematically consistent solution (e.g. continuous at $x = x_0$) we have *not* suppressed any possible instability, but always included it among the modes from the other side.

It is clear that the problem of the instability is still an open question.

V. Numerical examples

Numerical evaluation of the pressure field is not too difficult if we are able to find all the modal wavenumbers $\kappa_{m\mu}$ necessary for the required accuracy. We adopted the method, outlined in [7], which is based on continuation from the (assumed easily found) hard-wall values to the sought soft-wall values. The crux of the method is that we start from a suitable hard-wall direction $|Z| \to \infty$ in the complex impedance plane in order to capture all wavenumbers occurring at the finite impedance, say, Z_0. This is not entirely straightforward. When we trace the wavenumbers backwards, from the soft-wall to the hard-wall values, there are certain intervals of $\arg(Z)$ where some wavenumbers disappear to infinity. These would be impossible to find if we started there with our forward search. It transpires that a search along

[b] Incidentally, this case is taken from [8], where it is shown that the Briggs-Bers test does *not* decide the mode to be unstable.

vertical lines in the complex Z plane, from $Z = \mathrm{Re}(Z_0) - \mathrm{i}\infty$ when $M = 0$ and from $Z = \mathrm{Re}(Z_0) + \mathrm{i}\,\mathrm{sign}(M)\infty$ otherwise, guarantees finding of all the wave numbers.

To be completely specific, we define $Z_0 = R_0 + \mathrm{i}X_0$ and parameterise

$$\frac{1}{Y(\lambda)} = Z(\lambda) = R_0 + \mathrm{i}\delta\cot(\lambda), \quad 0 \le \lambda \le \lambda_0 = \mathrm{arccot}(\delta X_0), \tag{33}$$

where $\delta = \mathrm{sign}(M)$ if $M \neq 0$ and $\delta = -1$ if $M = 0$. Solutions κ for the hollow duct are now implicitly given for any λ by the identity

$$f(\kappa, Y) = Y E_m(\kappa) = \mathrm{i}\Omega^2 Y\, \mathrm{J}_m(\alpha) + \omega\alpha\, \mathrm{J}'_m(\alpha) \equiv 0. \tag{34}$$

We know the hard-wall solutions corresponding to $\lambda = 0$. After differentiation of f to λ we obtain an ordinary differential equation in κ that can be integrated numerically as an initial value problem. We thus pick a mode by choosing an initial value and solve numerically by standard methods

$$\frac{\mathrm{d}f}{\mathrm{d}\lambda} = \frac{\partial f}{\partial \kappa}\frac{\mathrm{d}\kappa}{\mathrm{d}\lambda} + \frac{\partial f}{\partial Y}\frac{\mathrm{d}Y}{\mathrm{d}\lambda} = 0 \tag{35}$$

to obtain an approximation for $\kappa(\lambda_0)$. If we deal with a surface wave, we divide f by J_m. The accuracy of the final result may be optimised by one or two Newton iterations. For an annular duct we do something similar with $f = Y_1 Y_h \mathcal{E}_m$.

The number of terms we need for $G_m(r, x)$ depends on the convergence rate. This depends greatly on the value of $x - x_0$, because the convergence is exponentially fast, through the occurring exponential $\exp(-\mathrm{i}\kappa_{m\mu}(x - x_0))$, whenever $x - x_0 \neq 0$. Only when $x = x_0$ the series converges conditionally when $r \neq r_0$ and (deceivingly) slowly diverges like a harmonic series ($\sim \mu^{-1}$) when $r = r_0$. It makes the series for G_m absolutely convergent and differentiable for any $x \neq x_0$, $r \neq r_0$, and just conditionally convergent and continuous at $x = x_0$, $r \neq r_0$. Unless we are very close to $r = r_0$, we will typically need here a few hundred terms for one percent accuracy. As the series at the left and right side of the source plane are not symmetric whenever $M \neq 0$, we will have a discontinuity at $x = x_0$ for any finite number of terms. Although this jump is a marked evidence of any insufficient accuracy, the absence of the jump is not always an indication of convergence. Also when M tends to zero the jump will disappear, but just by the solution becoming symmetric. It has no relation to the accuracy of the series.

To illustrate the points noted above, we present the $m = 3$-circumferential component G_m in figure 2 for a source at $x_0 = 0$, $r_0 = 0.7$ and $\omega = 10$ in an annular duct with $h = 0.3$, $Z_1 = 1 - \mathrm{i}$ and $Z_h = 1 + \mathrm{i}$ and a mean flow of $M = 0.5$. G_m is plotted at $r = 0.7$ for $-1 \le x \le 1$. In addition the complex axial wave numbers $\kappa_{m\mu}$ are presented. We observe two surface waves in the first quadrant, both candidate for instability. In order to make sure that the series has converged we used 400 radial modes, but the difference with less than that is only visible very near the source.

In addition to this example for annular ducts we have compared extensively our analytic Green's function for hollow ducts with the 'numerical' Green's function described by Alonso e.a..[5] We consider two cases, one with no mean flow, $M = 0$, and one with a typical 'intake' Mach number of $M = -0.45$. A typical non-dimensional frequency is $\omega = 28$ for the flow case and we choose $\omega = 31.354$ for the zero flow case so that the cut-on ratio is about the same for both cases. The impedance is $Z_1 = 2.5 - \mathrm{i}0$ in both cases. The number of cut-off modes initially assumed is 40 for both the analytical and numerical Green's function evaluation and only the positive modes 28 (-4) 0 are shown. The source position is always at the wall, $r_0 = 1$, and the observer position is also on the wall, $r = 1$, and at the same azimuthal location as the source but at a variable axial distance from the source both to the left and right of the source plane. The typical location of the axial wave numbers in the complex κ-plane for both cases is presented in figures 3. The presence of a very well cut-off surface wave in the case with flow anticipates the convergence problems to be reported below when the source is positioned at the wall, right inside the region where the surface wave is important.

For the first (zero flow) case, we show in Figure 4 the absolute value or modulus of each radial mode amplitude as a function of radial mode number: the figures on the left refer to the 'left running modes' i.e. the modes propagating outward from the source in the negative x direction, while the figures on the right refer to the 'right running modes', i.e. those propagating outward from the source in the positive x direction. The upper figures refer to our analytical Green's function, the lower figures to our evaluation of the mode amplitudes from the numerical Green's function.[5] In Figure 5 we show the corresponding mode amplitude phase results.

In this zero flow case, the analytical and numerical mode amplitudes agree to better than 10^{-14} and the mode amplitudes are the same for the left running modes as for the right running modes, as is the total field, a well-known result since the eigenvalues are identical, as illustrated in Figure 6. Here we have summed the radial modes for each azimuthal mode in the Green's function and plotted the axial variation of each azimuthal mode (modulus and phase) for a short distance to the left and right of the source plane, as well as the total Green's function (in both cases excluding

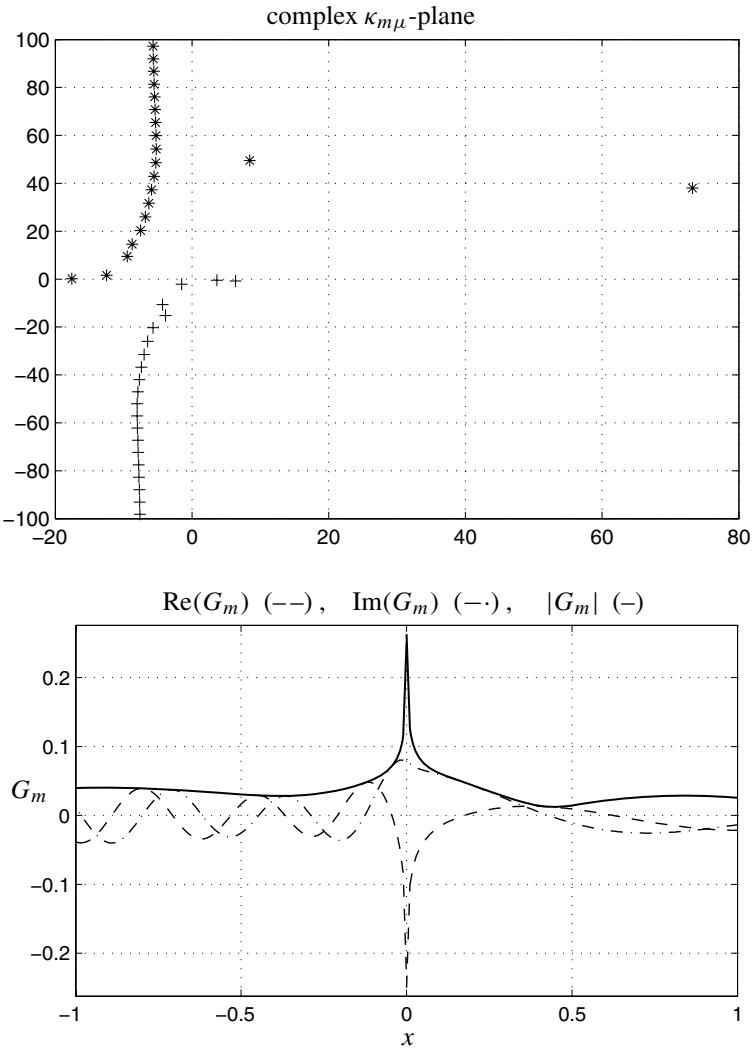

Figure 2. 400 modes at $r = r_0 = 0.7$ with $M = 0.5$, $\omega = 10$, $h = 0.3$, $m = 3$, $Z_1 = 1 - \mathrm{i}$, $Z_h = 1 + \mathrm{i}$

the constant factor $-(2\pi\mathrm{i})^{-1}$). Although these fields are the same on each side of source, this does not necessarily mean that we have a fully converged value at and near the source plane. This is demonstrated in Figure 7, where the same azimuthal quantities from both sides of the source plane are plotted as a function of the total number of radial modes included in each azimuthal mode for the analytical Green's function. It can be seen that none of the azimuthal mode amplitudes appear to have converged to a limit, at least not with the number of cut-off radial modes set at 40.

When we increase this number to a much higher number, say 200, we see, as in Figure 8, that convergence has been achieved (and in fact the left and right hand limits do agree as well) but if we require better than 1/2 dB accuracy we need something of the order of 200 modes. We cannot demonstrate this as easily with the numerical Green's function, as we have to invert, for each azimuthal mode number, a $2N \times 2N$ matrix where N is the number of radial modes. As we increase N much above 70, the matrix appears to become ill conditioned and we can no longer solve for the numerical mode amplitudes. However, below that limit the rate of convergence appears to be similar to that of the analytical Green's function.

For the flow case, the picture changes in some ways, in particular we have lost the left/right symmetry for the mode amplitudes, as shown in Figures 9 and 10. In Figure 11 we show the ratio of the analytical and numerical mode amplitudes and it can be seen that the two results agree to better than 20% in modulus for the cut-on modes although these differences appear to grow without limit for the very well cut-off modes. As a result the axial variation of the analytical and numerical Green's function agree fairly well away from the source plane, but at and near the source plane there are significant differences as shown in Figure 12, especially to the right of the source plane. Here there is

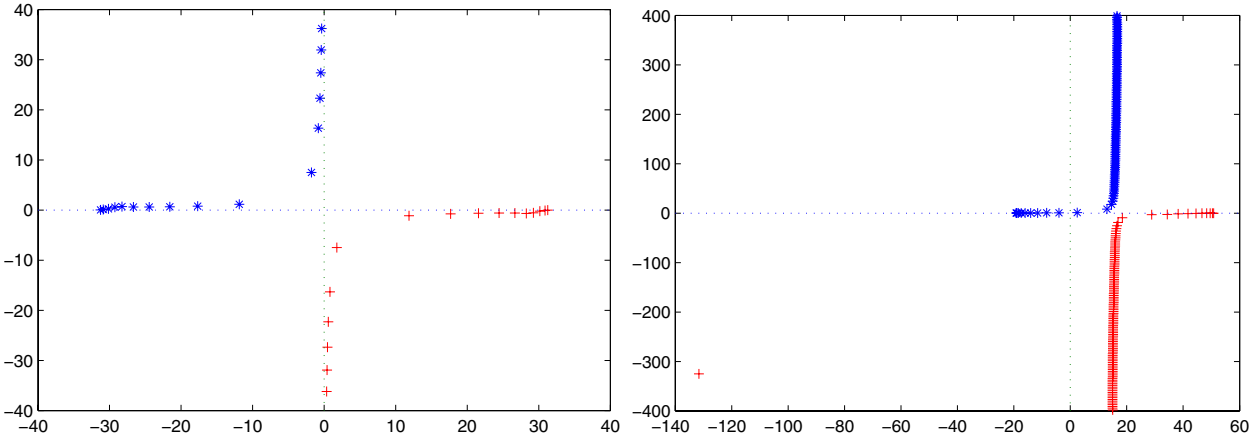

(a) $Z = 2.5$, $\omega = 31.354$, $m = 0$, $M = 0$ (b) $Z = 2.5$, $\omega = 28$, $m = 0$, $M = -0.45$

Figure 3. Location of $\kappa_{m\mu}$ for comparable no-flow and flow cases. Note with flow the very well cut-off surface wave, which yet plays a role near the wall around the source plane.

a larger discontinuity in the analytical Green's function than in the numerical one ($\sim$ 6 dB v. $\sim$ 3 dB).

However, with reference to the zero-flow case, if we increase the number of cut-off modes to 200 as before, the convergence behaviour is similar in some ways, but strikingly different for the modes to the right of the source plane as shown in Figure 13. Here there are dramatic jumps in the azimuthal mode amplitudes in the region of radial mode orders 80–95, which has been identified as the effect of a very well cut-off 'surface wave' which makes a large contribution at and near the duct wall (see figure 3). Once this has been included, the convergence is similar to the zero flow case. When this high number of radial modes is included in the analytical Green's function, the discontinuity at the source plane disappears as shown in Figure 14.

We therefore conclude that, provided a sufficient number of modes are included in the analytical Green's function, it does appear to exhibit continuity at the source plane. The agreement between the analytical and numerical Green's function is not as good as we would like for the non-zero flow cases we have investigated to date and our comparative testing of the two models will continue. But we suggest that, setting aside the possibility that we have not evaluated the numerical Green's function correctly, what seems to happening is this. The numerical Green's function with its enforced continuity at the source plane, when evaluated with an insufficient number of cut-off modes, attempts to achieve that continuity by slightly adjusting the amplitude of the cut-on modes and making larger adjustments to the well cut-off modes. If that is correct, when we proceed to evaluate the numerical Green's function with progressively larger numbers of radial modes, we should see a convergence of the numerical mode amplitudes to their analytical counterparts, for M not equal to zero.

A first step in that direction is shown in Figure 15, where we have increased the number of cut-off modes in the numerical Green's function from 40 to 70 and as in Figure 11 show the ratio of the analytical and numerical mode amplitudes for the same conditions as the flow case described above. In comparison with the ratios in Figure 11, Figure 15 shows ratios much closer to unity up to the highest mode number shown. This appears to confirm our suggestion that given sufficient cut-off modes the numerical Green's function amplitudes will converge, eventually, to those given by our analytical result.

VI. Conclusions

Since the duct modes are not known to be orthogonal or bi-orthogonal to any convenient set of basis functions, we did not derive the Green's function for time-harmonic sound waves in a lined circular duct with uniform mean flow in the usual way,[19] but by Fourier transformation. The found result takes the form of a common modal series.

The issue of a possible instability is still an open question. Causality considerations show mathematically, at least in the linear model, that some upstream running decaying modes are really downstream running instabilities. We have deliberately excluded this possibility from the examples, because the exponentially large fields that would result have little resemblance with physical reality. As there is no experimental evidence yet that the instability really exists, it may be an anomaly of the present model. Another possibility is that the experiments have not yet been able to detect

the associated nonlinearly saturated wave form.

Comparison of our analytical mode amplitudes (for the hollow duct version of our solution) with the numerical solution of Alonso e.a. showed a good agreement without mean flow, irrespective of how many modes are included in the matrix inversion for the numerical mode amplitudes. A large number of modes are required for convergence near the source. With flow, the mode amplitudes do not agree but as the number of modes included in the matrix inversion is increased the numerically obtained modal amplitudes of Alonso e.a. appear to be converging to the present analytical result. In addition, this numerical exercise showed the importance of including all relevant modes, especially when they behave as surface waves. When source and observer position are at the wall, they are in the regime of the surface wave, so irrespective of the modal decay rate, overlooking the surface wave produces an unconverged solution and a detectable discontinuity of the field at the source. A reliable method to find all modes, based on their behaviour with impedance Z along lines parallel to the imaginary axis is described in some detail.

VII. Acknowledgement

The contribution of SWR was partly carried out during a visit of the Department of Applied Mathematics and Theoretical Physics of the University of Cambridge, financed by a grant from the Royal Society, in the Spring of 2004. We are very grateful to both the Royal Society, the Department and Professor Nigel Peake for their support, hospitality, inspiring discussions and interest.

We are grateful to ms dr Heike JJ Gramberg and dr Nick C Ovenden for skillfully implementing the routine (34) to find all modal wave numbers. The present results would not have been possible without it.

References

[1] B.J. TESTER, N.J. BAKER, A.J. KEMPTON AND M.C.M. WRIGHT, 2004, Validation of an analytical model for scattering by intake liner splices, AIAA 2004-2906, 10th AIAA/CEAS Aeroacoustic Conference, Manchester, UK.

[2] A.M. CARGILL, 1993, Rolls-Royce Internal Report TSG0688.

[3] B.J. TESTER, 1973, The Propagation and Attenuation of Sound in Ducts Containing Uniform or "Plug" Flow. *Journal of Sound and Vibration* 28(2), 151–203.

[4] M.A. SWINBANKS, 1975, The sound field generated by a source distribution in a long duct carrying sheared flow, *Journal of Sound and Vibration* 40(1), 51–76.

[5] J.S. ALONSO and R.A. BURDISSO, 2003, Sound radiation from the boundary in a circular lined duct with flow, AIAA 2003-3144, 9th AIAA/CEAS Aeroacoustic Conference, Hilton Head, USA.

[6] J.S. ALONSO, L.R. MOLISANI and R.A. BURDISSO, 2004, Spectral and Wavenumber Approaches to Obtain Green's Functions for the Convected Wave Equation, AIAA 2004-2943, 10th AIAA/CEAS Aeroacoustic Conference, Manchester, UK.

[7] S.W. RIENSTRA, 2003, A Classification of Duct Modes Based on Surface Waves, *Wave Motion*, 37(2), 119–135.

[8] S.W. RIENSTRA and N. PEAKE, 2005, Modal Scattering at an Impedance Transition in a Lined Flow Duct, AIAA paper 2005-2852, 11th AIAA/CEAS Aeroacoustics Conference, Monterey CA, USA

[9] K.U. INGARD, 1959 Influence of Fluid Motion Past a Plane Boundary on Sound Reflection, Absorption, and Transmission. *Journal of the Acoustical Society of America* 31(7), 1035–1036.

[10] M.K. MYERS, 1980, On the Acoustic Boundary Condition in the Presence of Flow. *Journal of Sound and Vibration* 71(3), 429–434.

[11] M. ABRAMOWITZ and I.A. STEGUN, 1964, Handbook of Mathematical Functions, National Bureau of Standards, Dover Publications, Inc., New York.

[12] W. KOCH and W. MÖHRING, 1983, Eigensolutions for Liners in Uniform Mean Flow Ducts. *AIAA Journal* 21, 200–213

[13] A. BERS and R.J. BRIGGS, 1963, MIT Research Laboratory of Electronics Report No. 71 (unpublished)

[14] R.J. BRIGGS, 1964, *Electron-Stream Interaction with Plasmas*, Cambridge University Press, Cambridge

[15] A. BERS, 1983, Space-time evolution of plasma instabilities-absolute and convective, *Handbook of Plasma Physics*, edited by M.N. Rosenbluth and R.Z. Sagdeev (North-Holland, Amsterdam), Vol. I, p. 451.

[16] D.G. CRIGHTON and F.G. LEPPINGTON, 1974, Radiation Properties of the Semi-Infinite Vortex Sheet: the Initial-Value Problem, *Journal of Fluid Mechanics* 64(2), 393–414.

[17] D.S. JONES and J.D. MORGAN, 1972, The Instability of a Vortex Sheet on a Subsonic Stream under Acoustic Radiation, *Proc. Camb. Phil. Soc.* 72, 465–488.

[18] S.W. RIENSTRA, 1988, "1D Reflection at an Impedance Wall", *Journal of Sound and Vibration*, 125, 43–51

[19] G.F. ROACH, 1982, Green's Functions. Cambridge University Press, Cambridge.

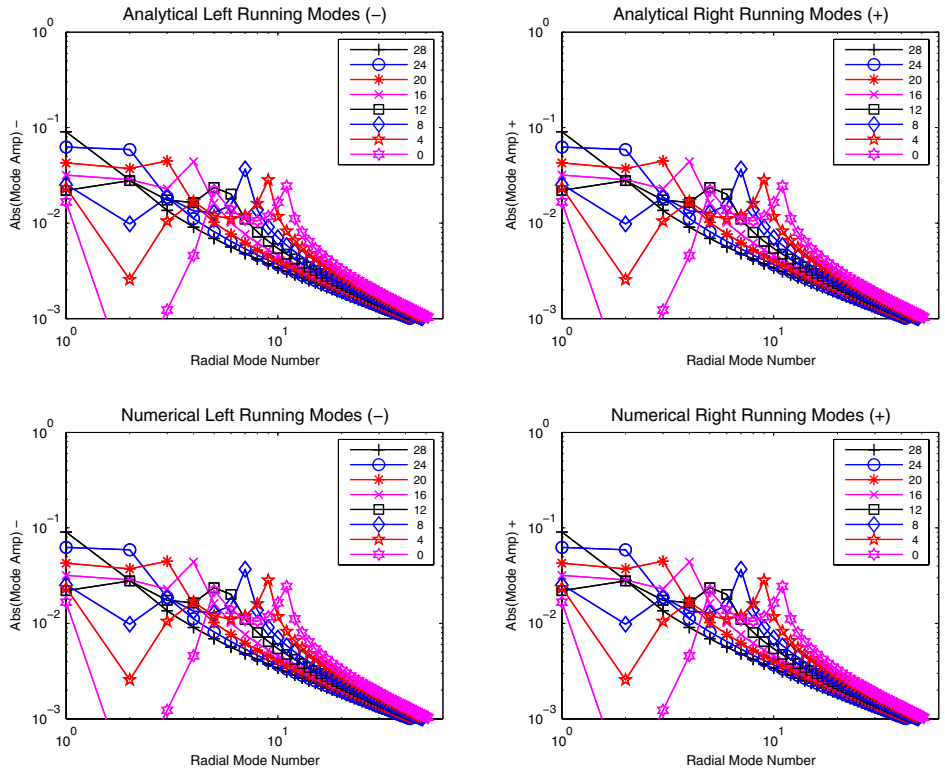

Figure 4. Analytic v. numerical Green's function mode amplitude: modulus ($\omega = 31.354$, $M = 0$, $Z_1 = 2.5$, $r_0 = 1$, **40 cut-off modes).**

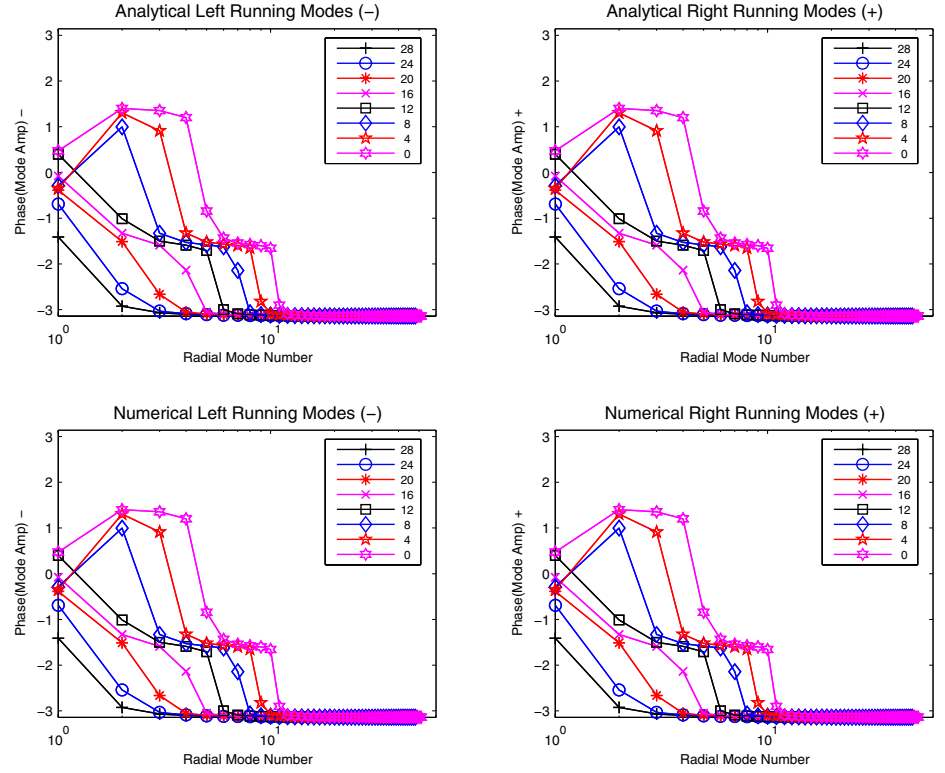

Figure 5. Analytic v. numerical Green's function mode amplitude: phase ($\omega = 31.354$, $M = 0$, $Z_1 = 2.5$, $r_0 = 1$, **40 cut-off modes).**

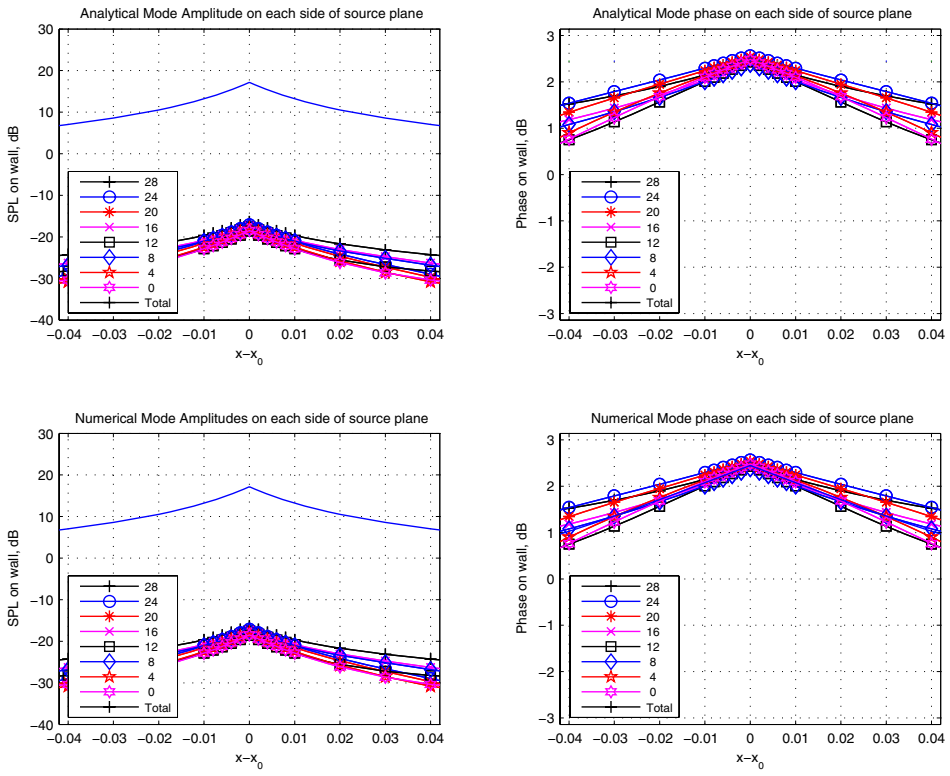

Figure 6. Axial variation of analytic and numerical Green's function azimuthal mode amplitudes ($\omega = 31.354$, $M = 0$, $Z_1 = 2.5$, $r_0 = 1$, **40 cut-off modes).**

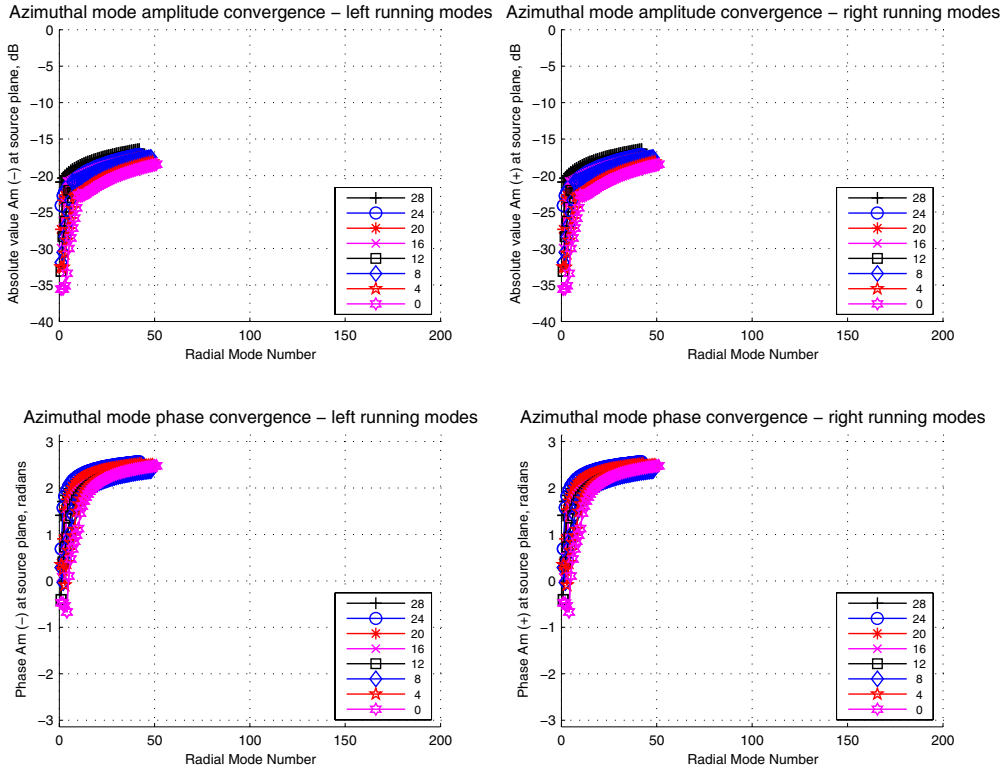

Figure 7. Analytic Green's function azimuthal mode amplitude convergence ($\omega = 31.354$, $M = 0$, $Z_1 = 2.5$, $r_0 = 1$, **40 cut-off modes).**

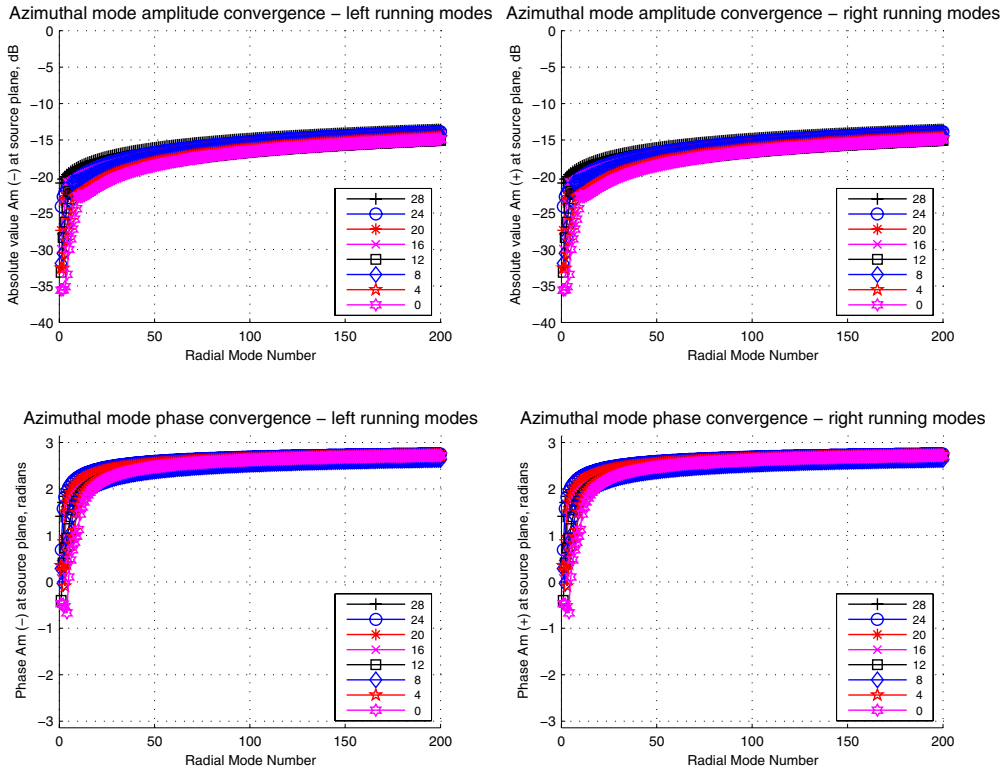

Figure 8. Analytic Green's function azimuthal mode amplitude convergence ($\omega = 31.354$, $M = 0$, $Z_1 = 2.5$, $r_0 = 1$, **200 cut-off modes).**

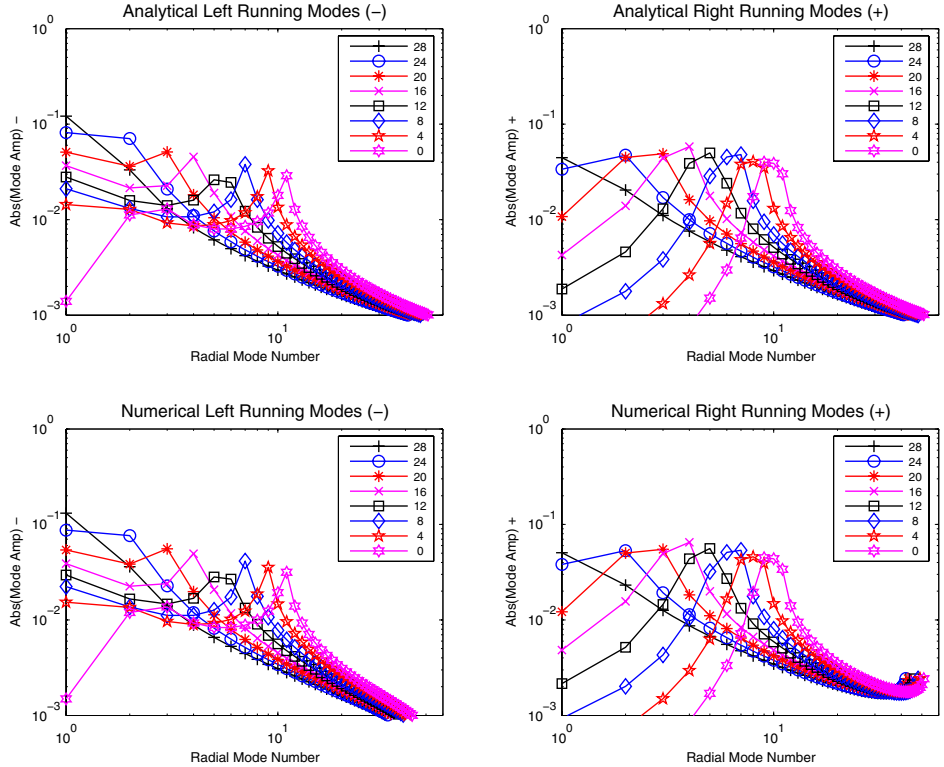

Figure 9. Analytic v. numerical Green's function mode amplitude: modulus ($\omega = 28$, $M = -0.45$, $Z_1 = 2.5$, $r_0 = 1$, **40 cut-off modes).**

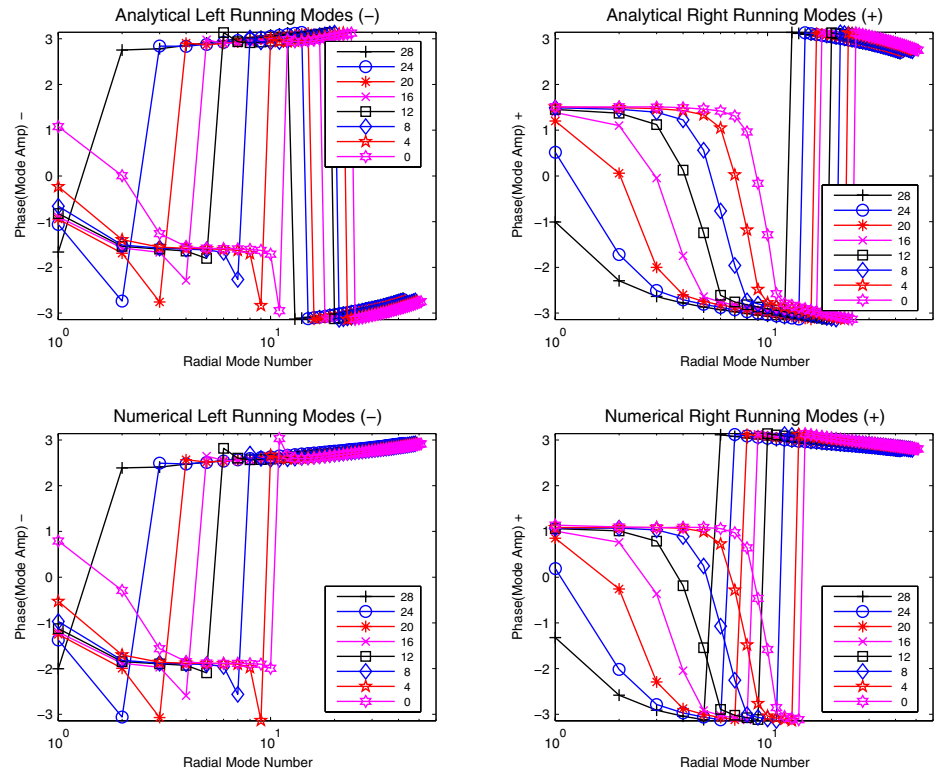

Figure 10. Analytic v. numerical Green's function mode amplitude: phase ($\omega = 28$, $M = -0.45$, $Z_1 = 2.5$, $r_0 = 1$**, 40 cut-off modes).**

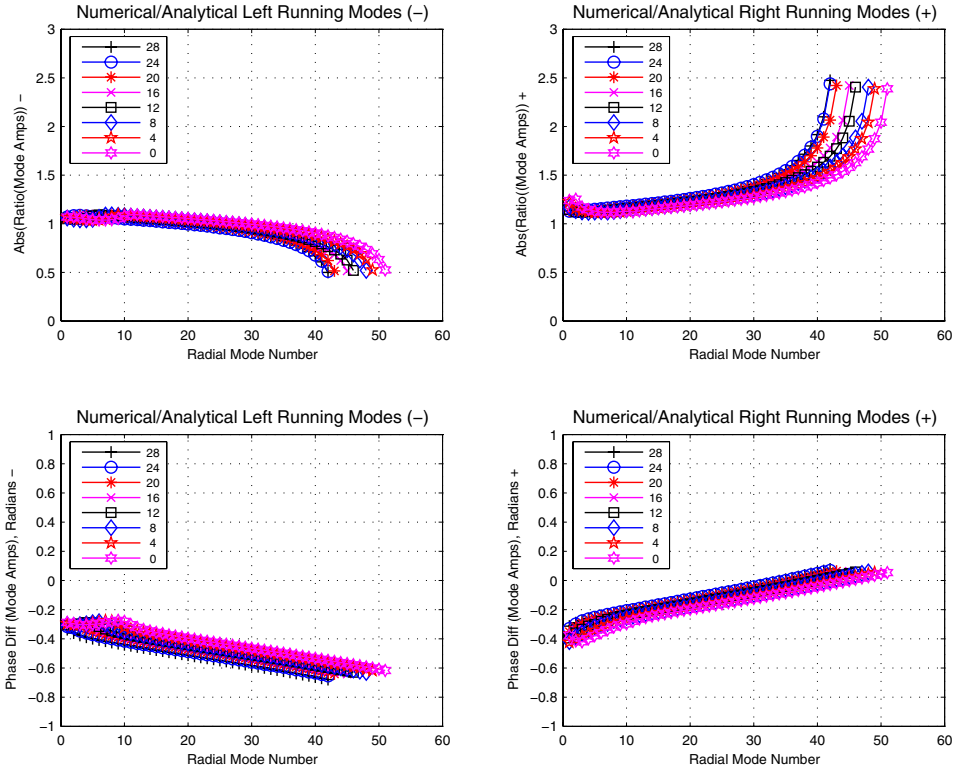

Figure 11. Ratio of analytic and numerical Green's function mode amplitudes ($\omega = 28$, $M = -0.45$, $Z_1 = 2.5$, $r_0 = 1$**, 40 cut-off modes).**

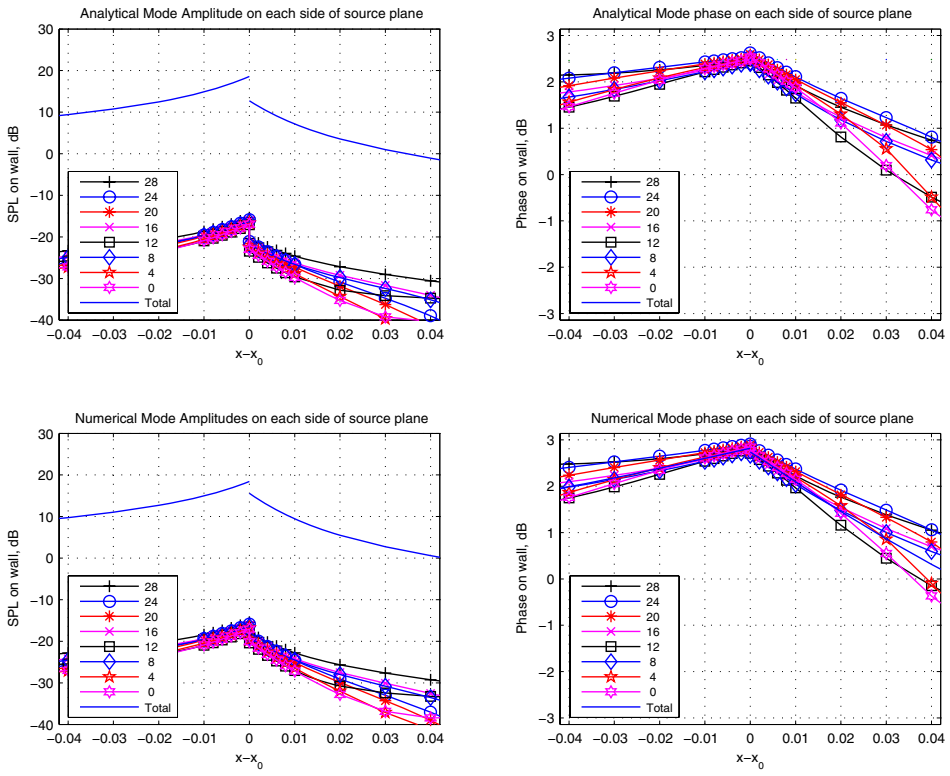

Figure 12. Axial variation of analytic and numerical Green's function azimuthal mode amplitudes ($\omega = 28$, $M = -0.45$, $Z_1 = 2.5$, $r_0 = 1$, **40 cut-off modes).**

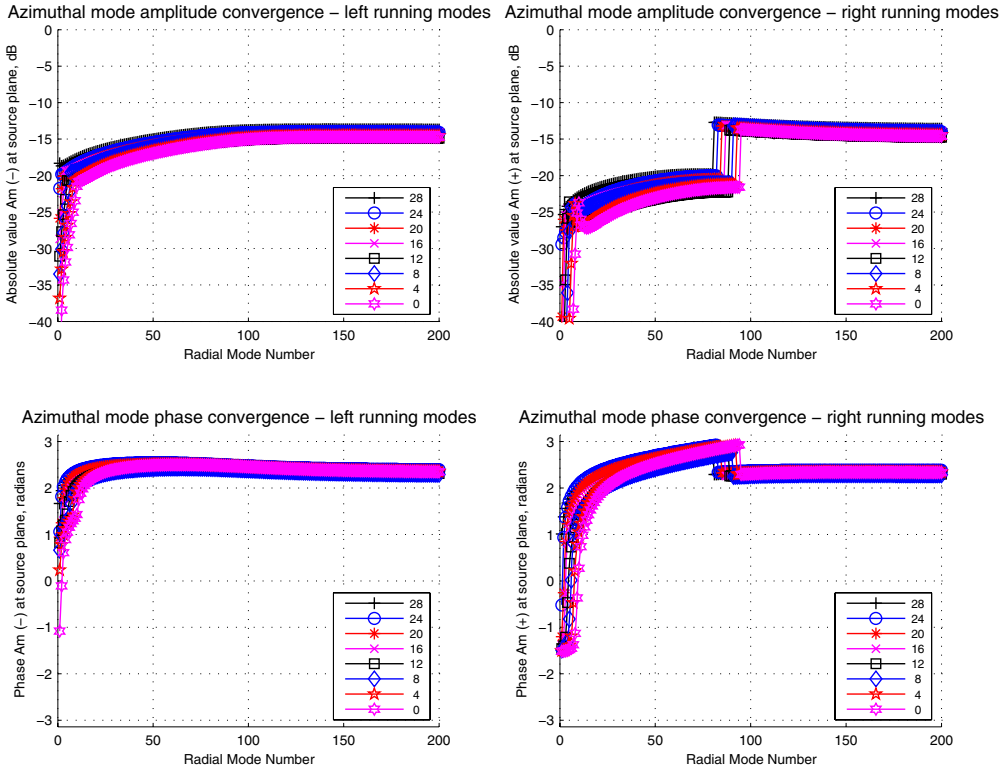

Figure 13. Analytic Green's function azimuthal mode amplitude convergence ($\omega = 28$, $M = -0.45$, $Z_1 = 2.5$, $r_0 = 1$, **200 cut-off modes).**

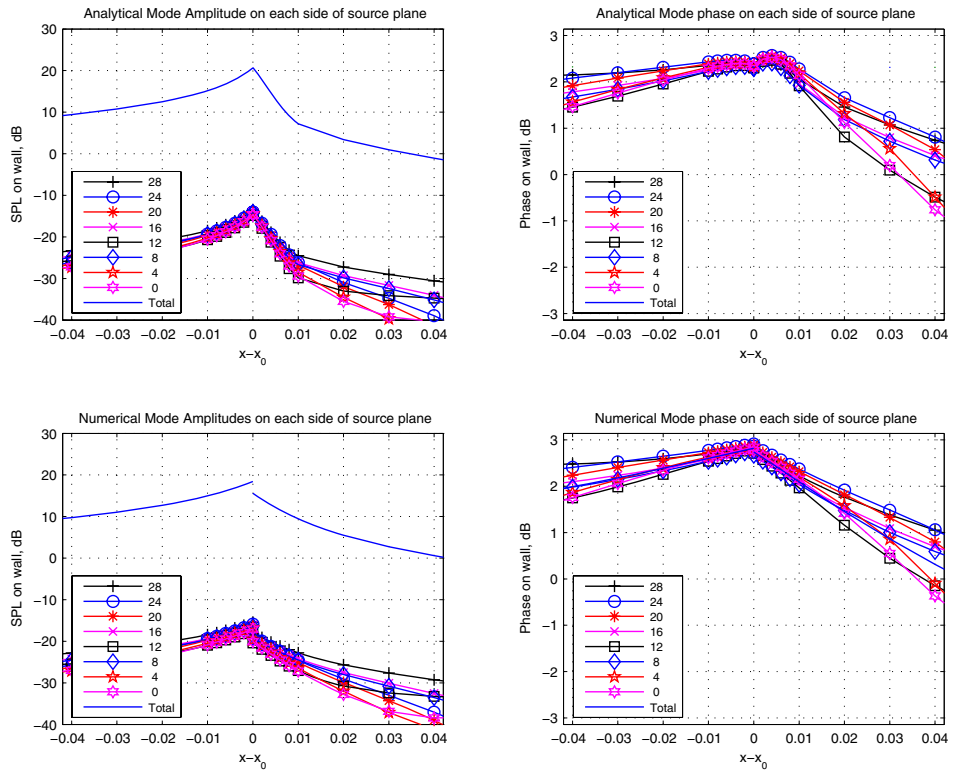

Figure 14. Axial variation of analytic and numerical Green's function azimuthal mode amplitudes ($\omega = 28$, $M = -0.45$, $Z_1 = 2.5$, $r_0 = 1$, **200 cut-off modes for analytical, 40 for numerical).**

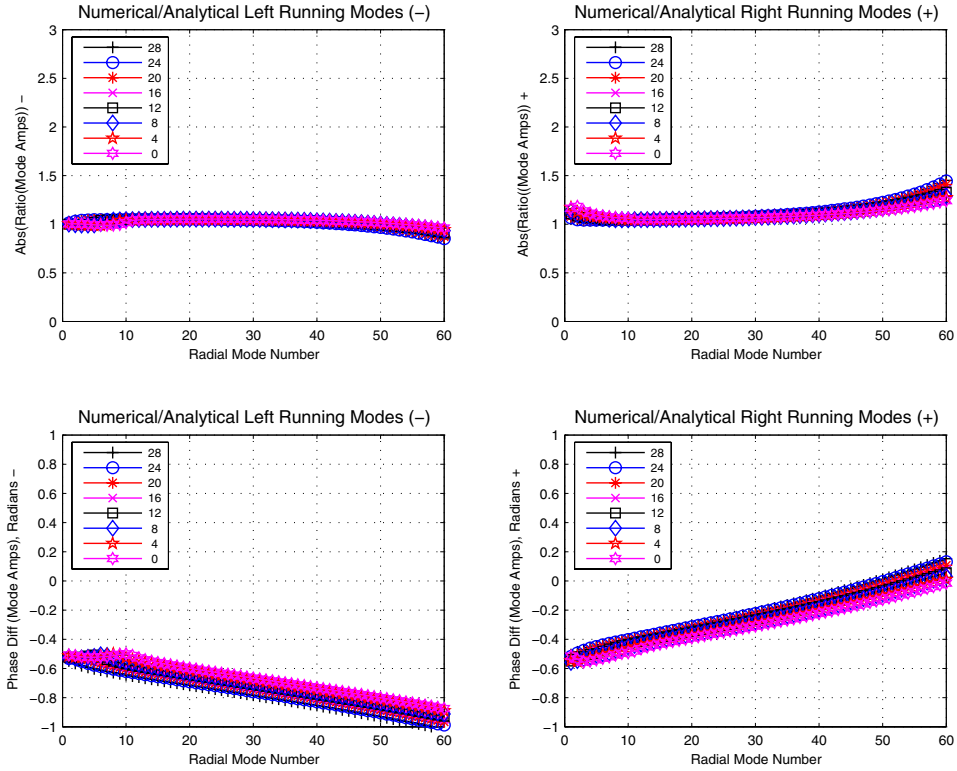

Figure 15. Ratio of analytic and numerical Green's function mode amplitudes ($\omega = 28$, $M = -0.45$, $Z_1 = 2.5$, $r_0 = 1$, **70 cut-off modes).**